Intercalation of polyethylene oxide PEO in layered MPS_3 (M = Ni, Fe) materials

V. Manríquez[a,*], P. Barahona[a], D. Ruiz[a], R.E. Avila[b]

[a]*Departamento de Química, Facultad de Ciencias, Universidad de Chile,*
Casilla 653, Santiago, Chile
[b]*Departamento de Investigación y Desarrollo,*
Comisión Chilena de Energía Nuclear, Casilla 188-D, Santiago, Chile

Abstract

The intercalation compounds $Li_{0.96}(H_2O)_{0.77}(PEO)_{0.63}Ni_{0.48}PS_3$ and $Li_{0.94}(H_2O)_{0.92}(PEO)_{0.94}Fe_{0.48}PS_3$ obtained by the insertion of PEO in MPS_3 form lithium-polyethylene oxide complexes containing Li^+ exchangeable cation in the interlayer space. Polyethylene oxide (PEO) is able to associate interlayer cation increasing the ionic conductivity of $NiPS_3$ and $FePS_3$. These compounds constitute a new family of intercalates MPS_3 (M = Ni, Fe) host-layer materials.

The new materials were characterized by powder X-Ray diffraction (XRD), Fourier-transformed infrared (FT-IR), differential thermal and thermogravimetric analyses (DTA/TG), energy dispersive X-Ray (EDX), inductively coupled plasma (ICP) and electrochemical impedance measurements. The intercalation compound $Li_{0.96}(H_2O)_{0.77}(PEO)_{0.63}Ni_{0.48}PS_3$ shows an ionic conductivity of 0.13 μS/cm, and dc electronic conductivity of ca. 0.1 μS/cm which is twice that of $NiPS_3$.

* Corresponding author. Tel.: +56 2 6787 251; fax: +56 2 2713 888.
E-mail address: vmanriqu@abello.dic.uchile.cl (V. Manríquez).

1. Introduction

Increasing interest in the intercalation of organic polymers in layered inorganic host materials to form organic/inorganic nanostructure systems is due to a very specific physical and chemical behavior synergistically derived from both host and guest [1].

The intercalation of polyethylene oxide, $(C_2H_4O)_n$, associated with interlayer cations into a layered inorganic host produces a two-dimensional material comprising alternating layers of organic PEO and inorganic sheet structures with enhanced electrical properties. PEO can also be intercalated between layered inorganic hosts, such as montmorillonite [2], V_2O_5 [3], MS_2 (M = Mo, Ti) [4], MoO_3 [5] and MPS_3 (M = Mn, Cd) [6].

Transition metal chalcogenophosphates MPS_3 have been extensively studied because of their interesting electrical properties and their application as cathode materials for rechargeable high-energy–density lithium batteries. Among the chalcogenophosphate that have been tested, $NiPS_3$ and $FePSe_3$ behave as promising cathode materials [7]. Electrochemical studies near thermodynamic equilibrium have indicated an insertion limit close to 1.5 lithium atoms/$NiPS_3$ [8].

We have previously reported the insertion of trivalent cations and polyaniline into MPS_3 (M = Mn, Cd) by a cation transfer mechanism based on the ability of these materials to exchange a fraction of the M^{+2} intralayer cations by cations from aqueous solutions, and measured the physical properties of the products [9,10].

The present work describes innovative preparation routes for the intercalation of organic polymers into layered MPS_3 (M = Ni, Fe) host material. The objective is to obtain intercalated materials that combine the electronic behavior of a semi-conducting host lattice with the ionic-conductivity properties of PEO/alkali-metal guest species. We report here the preparation and characterization of polyethylene oxide intercalate in lamellar MPS_3 (M = Ni, Fe).

2. Experimental

2.1. Preparation of host compounds

The intermediate compounds Li_xMPS_3 were prepared by reaction of the high-purity elements (99.9%) P, M (M = Ni, Fe) and Li_2S, supplied by Aldrich, in stoichiometric amounts; the reaction mixtures were sealed in evacuated quartz tubes and then heated at 1023 K for 1 week. After the reaction was complete, the product was slowly cooled to room temperature. SEM-EDX analysis carried out on the intermediate compounds confirmed their purity, homogeneity and stoichiometry (Table 1).

Table 1
Analytical data for LiM_xPS_3 and $Li(H_2O)_y(PEO)_zM_xPS_3$ (M = Ni, Fe) nanocomposites

Compounds	H_2O	$(PEO)_n$	Analytical data (%, w/w)						
	Δm (%)	Δm (%)	Li	Ni	Fe	P	S	C	H
$Li_{0.96}Ni_{0.48}PS_3$	–	–	4.2	17.6	–	19.3	58.7	–	–
$Li_{0.96}(H_2O)_{0.77}(PEO)_{0.63}Ni_{0.48}PS_3$	8.5	16.9	3.3	13.9	–	15.3	47.0	7.5	1.2
$Li_{0.94}Fe_{0.48}PS_3$	–	–	4.1	–	16.8	19.4	59.5	–	–
$Li_{0.94}(H_2O)_{0.92}(PEO)_{0.94}Fe_{0.48}PS_3$	8.0	19.0	3.0	–	12.3	14.2	43.8	10.4	1.7

2.2. *Preparation of intercalated compounds*

To swell the layers apart, we form in a first step, hydrated Li_xMPS_3 phases from an aqueous suspension. The intercalation of PEO was achieved by treatment the intermediates $Li_{0.96}(H_2O)_{x-}Ni_{0.48}PS_3$, or $Li_{0.94}(H_2O)_xFe_{0.48}PS_3$ with a water/acetonitrile (1/4) solution of PEO (Aldrich, molecular weight of 10^5 a.m.u.) under vigorous shaking for 24 h at room temperature. The resulting products were washed with acetonitrile and vacuum-dried. The stoichiometry of the final products was determined by both elemental and thermogravimetric analysis (Table 1).

2.3. *Characterization*

The powder XRD data were collected at room temperature on a Siemens D-5000 powder diffractometer, with Cu Kα radiation in the range of $5 < 2\theta < 60$. Elemental analysis was obtained by energy-dispersive X-ray EDX and ICP-Plasma for all compounds described here. SEM-EDX analyses were obtained on a CAMECA SU 30 system with Princeton Gamma detector. Differential thermal analysis (DTA) and thermogravimetric analysis (TGA) were performed on a STA 1500H/625 thermal analysis system, Rheometric Scientific. The DTA/TG curves were obtained simultaneously on each sample from room temperature to 1273 K in flowing nitrogen, using a heating rate of 10 K/min.

Infrared spectra were obtained in the range $500–1500 \text{ cm}^{-1}$ on samples pressed into KBr disks, using a Bruker VECTOR 22 system with Fourier-transformed SJ-IR spectrometer.

Electrical properties of the samples were measured by ac and dc methods on cylindrical disk samples, mounted between two gold electrodes. The ac conductivity measurements were carried out by ac complex impedance analysis in the frequency range from 0.01 to 10 MHz using a Solartron SI-1260 impedance/gain phase analyser with signal levels from 0.2 to 1 V. Direct current dc conductivity was determined by a Keithley 237 source-meter.

3. Results and discussion

The kinetics of intercalation of organic polymers into layered compounds is generally unfavorable due to the high activation energy associated with the deformation of the crystal structure of the inorganic host. Thus, the insertion process requires the expansion of the interlayer spacing by previous intercalation of a simple small hydrated ion [11].

The reaction of the pure elements P, S, M (M = Ni, Fe) and Li_2S forms the phases $Li_{0.96}Ni_{0.48}PS_3$ and $Li_{0.94}Fe_{0.48}PS_3$. We tested the relation between different hydratations grade of the Li_xMPS_3 phases with the interlayer distance. The Fig. 1 shows XRD patterns of $Fe_{0.98}PS_3$, $Li_{0.94}Fe_{0.48}PS_3$, $Li_{0.94}(H_2O)_{1.01-}Fe_{0.48}PS_3$ and $Li_{0.94}(H_2O)_{2.80}Fe_{0.48}PS_3$ (the compounds with Ni are similar). The similarity of XRD patterns of $Fe_{0.98}PS_3$ and $Li_{0.94}Fe_{0.48}PS_3$ is apparent. However, due to the relatively large solvation energy of the lithium cation, extensive hydration results in an influx of water molecules that expands the interlayer distance from 6.4 (unhydrated phase) to 12.0 Å (completely hydrated phase). The latter also indicates that the lithium ion lies in the interlayer space in both compounds.

The $Li(H_2O)_x(PEO)_yNi_{0.5}PS_3$ nanocomposites were obtained by reaction of the intermediates $Li(H_2O)_xM_{0.5}PS_3$ (M = Ni, Fe) with PEO. The stoichiometry of the final product $Li_{0.96}(H_2O)_{0.77}(PEO)_{0.63}Ni_{0.48}PS_3$ (compound I) and $Li_{0.94}(H_2O)_{0.92}(PEO)_{0.94}Fe_{0.48}PS_3$ (compound II) was determined
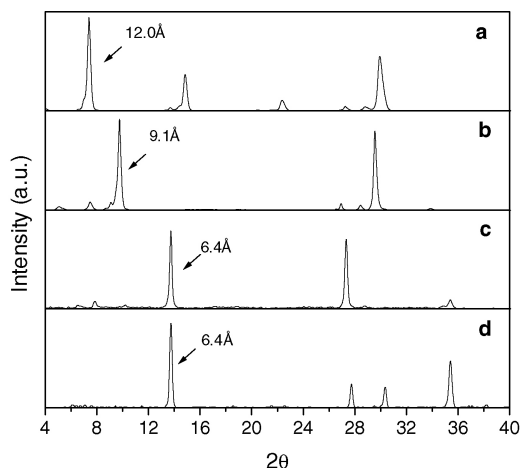
Fig. 1. Powder X-ray diffractions patterns of (a) $Li_{0.94}(H_2O)_{2.80}Fe_{0.48}PS_3$, (b) $Li_{0.94}(H_2O)_{1.01}Fe_{0.48}PS_3$, (c) $Li_{0.94}Fe_{0.48}PS_3$, and (d) $Fe_{0.98}PS_3$.

by elemental and thermogravimetric analysis (Table 1); slight deviations from the ideal composition may reflect some heterogeneity of the samples. Compound I show mass losses of 8.5 and 16.9% below 200 and 300 °C, respectively (Fig. 2) whereas compound II show mass losses of 8 and 20.2% in the same temperature range. These weight losses from the two nanocomposites are ascribed to dehydration and PEO decomposition, respectively. The organic contents derived from the DTA/TG measurements are 6% larger than those obtained from elemental analyses, which suggests some degradation of the inorganic structure below 600 °C. The materials are thermally stable under nitrogen up to 200 °C in the case of compound I, and 205 °C in the case of compound II.

The intercalated compounds were characterized by X-ray powder diffraction. The XRD patterns of the intercalate compounds show a significant loss of crystallinity; the sharp 0 0 1 reflections yield an
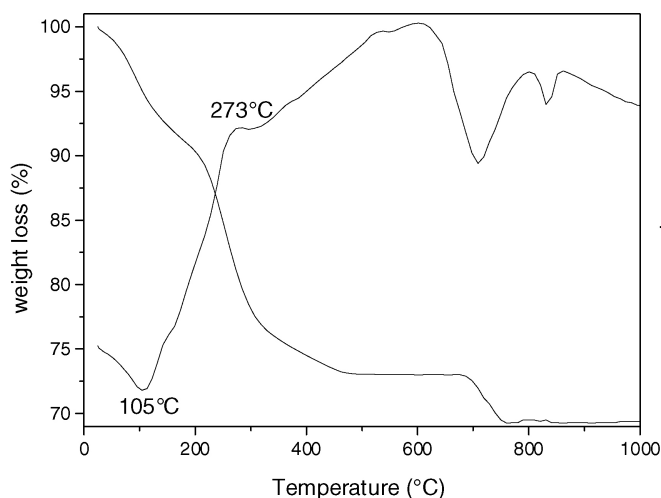

Fig. 2. Simultaneous DTA/TG for $Li_{0.96}(H_2O)_{0.77}(PEO)_{0.63}Ni_{0.48}PS_3$.
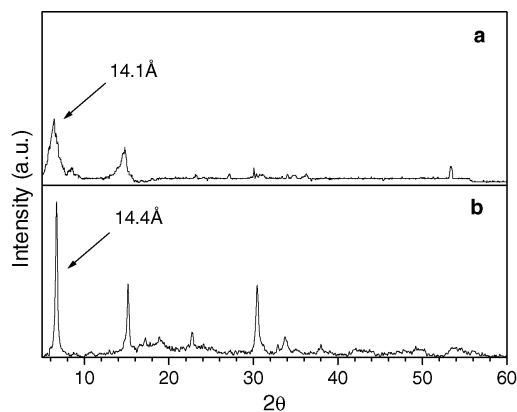
Fig. 3. Powder X-ray diffractions patterns of (a) $Li_{0.94}(H_2O)_{0.92}(PEO)_{0.94}Fe_{0.48}PS_3$ and (b) $Li_{0.96}(H_2O)_{0.77}(PEO)_{0.63}Ni_{0.48}PS_3$.

interlamellar distance of 14.4 and 14.1 Å for compounds I and II, respectively (Fig. 3). The increase in basal spacing compared with pristine MPS_3 can be interpreted as the intercalation of PEO either with helical conformation, or as a two-layer arrangement of PEO chains in a zigzag conformation.

The experimental stoichiometry is around 0.7 CH_2CH_2O units per $LiNi_{0.5}PS_3$ formula and 1.0 CH_2CH_2O units per $LiFe_{0.5}PS_3$ suggesting that the arrangement is less dense than a double layer of linear, zigzag-like PEO chains. FT-IR spectra of the intercalates (Fig. 4) show some characteristic bands attributed to CH_2CH_2O groups (Table 2) and display two strong bands at 605 and 555 cm^{-1} arising from the splitting of the $\nu(PS_3)$ stretching band at 570 cm^{-1} in $NiPS_3$. The splitting reflects the presence of intralamellar guest species [12]. The peaks observed in the 1500–800 cm^{-1} region for pure PEO are not
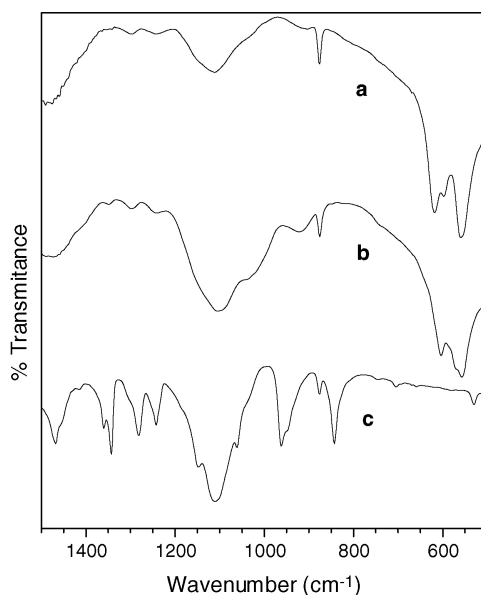

Fig. 4. FT-IR spectra of (a) $Li_{0.96}(H_2O)_{0.77}(PEO)_{0.63}Ni_{0.48}PS_3$, (b) $Li_{0.94}(H_2O)_{0.92}(PEO)_{0.94}Fe_{0.48}PS_3$, and (c) PEO.

Table 2
IR spectra assignments of $Li_{0.94}(H_2O)_{0.92}(PEO)_{0.94}Fe_{0.48}PS_3$, $Li_{0.96}(H_2O)_{0.77}(PEO)_{0.63}Ni_{0.48}PS_3$ and pure polyethylene oxide

PEO frequency (cm^{-1})	$Li_{0.94}(H_2O)_{0.92}$ $(PEO)_{0.94}Fe_{0.48}PS_3$ frequency (cm^{-1})	$Li_{0.96}(H_2O)_{0.77}$ $(PEO)_{0.63}Ni_{0.48}PS_3$ frequency (cm^{-1})	Assignment [12]
1468	1474	1491	CH$_2$
1343	–	–	CH$_2$
1281	1298	1298	CH$_2$
1242	1242	1242	CH$_2$
1111	1105	1111	C–O
876	876	876	CH$_2$

well defined in intercalated PEO. The absence of the band characteristic of vibrations of *trans* O–(CH$_2$)$_2$–O groups at 1305 cm^{-1} (present in zigzag conformation) may indicate a helical conformation for PEO [5].

Both XRD and IR data confirm the intercalation of PEO in NiPS$_3$ and FePS$_3$ host matrixes. Thus, the PEO chains solvating the Li$^+$ ion may exhibit a helical structure similar to that found in the corresponding PEO intercalates in MPS$_3$ (M = Mn, Cd) [6] and to the PEO–lithium salt solid electrolytes [13]. It is reasonable to assume that solvation of the Li$^+$ ion by the oxygen atoms of the polyethylene oxide is the driving force of the polymer insertion process.

Impedance data of pellets 1 mm in thickness and 6.7 mm in diameter were obtained at room temperature in the 0.01 Hz to 10 MHz range, with an ac signal of 250 mV. Typical impedance complex plane plots show a single depressed arc, followed by low-frequency arc, or a constant phase spike, as shown in Fig. 5. The high-frequency arc (HFA) can be fit [14] with the parallel combination of a resistor and a constant phase element (CPE), of which the admittance is

$$Y_{CPE} = Y_o(j\omega)^n$$

Thus, the impedance data of compound II (Fig. 5a) can be fit with a CPE in series with the parallel combination of a resistor and a second CPE with a goodness-of-fit χ^2-value of 5×10^{-4}. In this fit, the first CPE is associated with the low-frequency spike, with the parameters $Y_{o1} = 14(2)$ nF(s)$^{n-1}$ with $n_1 = 0.55(1)$. The R–CPE$_2$ parallel combination fits the depressed HFA with the values $R = 788(3)$ kΩ, $Y_{o2} = 4.67(3)$ pF(s)$^{n-1}$, with $n_2 = 0.673(3)$. From the latter parameters of CPE$_2$, and using the expression $C = Y_o (\omega_{max})^{n-1}$ [15] with $f_{max} = 22.5$ kHz, the value 8.85 pF follows for the corresponding capacitance.

The fitting of CPE$_1$ to a low-frequency constant phase spike with a value of n close to 0.5 suggest ascribing that feature to a diffusion-related surface-electrode process. However, extraction of diffusion parameters may be premature, given the layered composition of the material, which allows for other charge displacement processes within the bulk to cause the observed behavior.

In compound I (Fig. 5b), an HFA (10 MHz–100 kHz) (Fig. 5c) is followed by a low-frequency arc down to 0.04 Hz. These data have been fit with the series combination of two parallel resistor-CPE elements, to a goodness-of-fit χ^2-value of 1.15×10^{-3}. The parameters of CPE$_1$, corresponding to the HFA are $Y_{o1} = 34(5)$ nF(s)$^{n-1}$ with $n_1 = 0.606(9)$, $f_{max} = 3$ MHz (corresponding to a $C_1 = 47(6)$ pF capacitor) and $R_1 = 1.086(8)$ kΩ. The low-frequency arc is fit by $Y_{o2} = 1.69(1)$ µF(s)$^{n-1}$ with $n_2 = 0.741(2)$, $f_{max} = 0.024$ Hz (corresponding to a $C_2 = 2.76(2)$ µF capacitor) and $R_2 = 2.12(6)$ MΩ. This value of the capacitance suggests assigning this low-frequency arc to an electrode interface process.
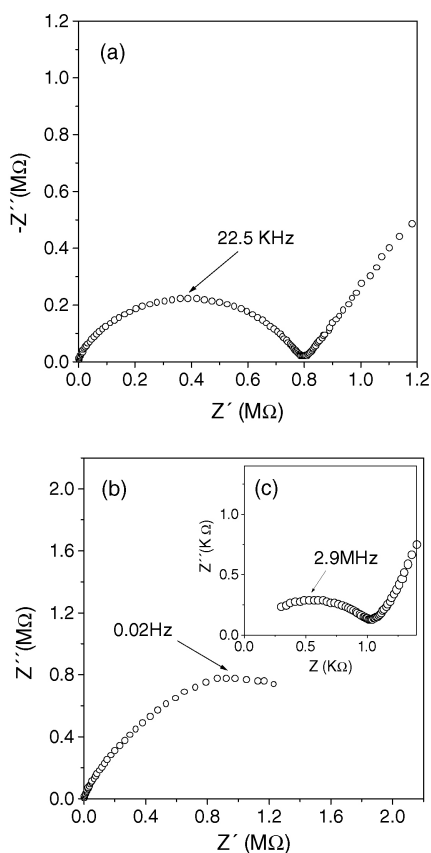
Fig. 5. Impedance plot for (a) $Li_{0.94}(H_2O)_{0.92}(PEO)_{0.94}Fe_{0.48}PS_3$, and (b and c): $Li_{0.96}(H_2O)_{0.77}(PEO)_{0.63}Ni_{0.48}PS_3$.

Considering further that no rectification appears in the residual electronic transport revealed by dc I–V curves, the transport process responsible for the low-frequency arc should be of ionic kind. Thus, an assignment to ionic electrode polarization is proposed leading to a value of $0.13 \, \mu S/cm$ for the effective ionic conductivity.

If the HFA of the Nyquist diagrams is ascribed to the bulk transport process, the values of the corresponding capacitance would imply relative permittivity values of 149 and 28 in compounds I and II, respectively. These values are unexpectedly high for the bulk material, so an assignment to the intergrain process seems reasonable [11,16]. However, the latter would imply the existence of an arc, or resistance offset from the origin caused by the bulk contribution. The absence of either of the present measurements may be an indication that the bulk conductivity leads to a high-frequency resistance no higher than the corresponding uncertainty, i.e., some $100 \, \Omega$ in compound I, or $1 \, k\Omega$ in compound II.

Further interpretations require identifying the current paths and ''grains'' regarding electronic and ionic transport in these compounds. Considering the layered structure described above, it is assumed that (i) the electronic transport is efficient along the layers, but nearly absent in the perpendicular direction; then, pieces of layers constitute the grains for electronic transport, grain boundaries being the regions between piece edges and (ii) ionic transport occurs along a connected network of interlayer regions without grain boundaries.

Further, assuming electronic mobilities much higher than ionic mobilities and electrodes that are ohmic for electronic transport but blocking to the ionic contribution, the high frequency and dc behavior are assumed dominated by electronic transport. At low and intermediate frequencies, the ionic contribution may dominate by electrode polarization in particular at low frequency. The electronic conductivity is affected also by the notorious preferential alignment of the layers in the direction perpendicular to the current path. A rough expectation on the resulting effective electronic conductivity is several orders of magnitude higher than the gross dc conductivity of the compound, since by far, the largest contribution to the gross dc resistance is the intergrain resistance.

The effective electronic conductivity corresponds, in this model, to the high-frequency "bulk" conductivity and its value determines whether or not the bulk arc may be unreachable to the equipment used, $100–1000\ \Omega$ from the impedance origin. Lacking an estimate for that value, the HFA cannot be ascribed to either the bulk or intergrain transport processes.

Comparing the data from the two composites, the larger capacitance and smaller resistance values in compound I may be caused by a larger electronic carrier density, if the HFA is due to electronic intergrain transport. This interpretation assumes that the capacitance is due to carrier accumulation/depletion layers at these boundaries, leading to a value proportional to the reciprocal of that layer thickness. Following that reasoning, it is possible that the low-frequency constant phase spike in the latter composite would evolve into an arc at much lower frequencies than experimentally possible with the present equipment.

Regarding the dc conductivity, current–voltage measurements taken by sweeping the bias at a constant rate in the range of -1 to $+1$ V result in an essentially ohmic response, shifted towards positive current when crossing $V = 0$, which is understood as derived from ionic or electronic trap activity which lags the bias.

The latter suggestion has been tested by measuring long-term (20 min–12 h) current transients during and following a bias pulse (of 100 mV). As seen in Fig. 6, during the bias pulse in compound I a sharp
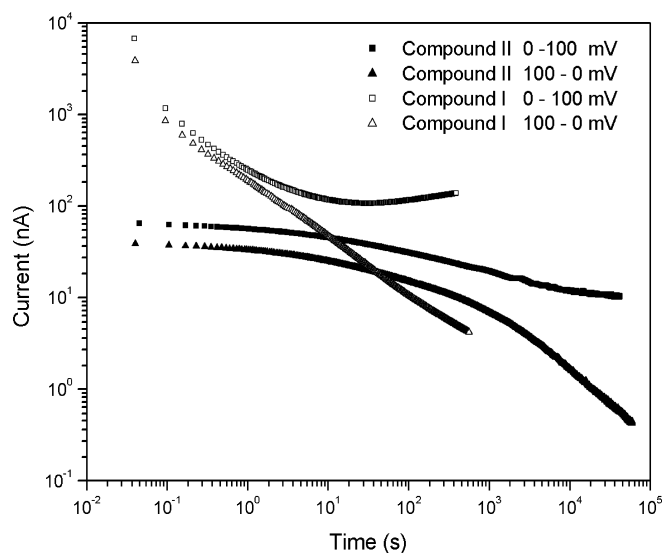

Fig. 6. Current–voltage plot for $Li_{0.94}(H_2O)_{0.92}(PEO)_{0.94}Fe_{0.48}PS_3$ (compound II) and $Li_{0.96}(H_2O)_{0.77}(PEO)_{0.63}Ni_{0.48}PS_3$ (compound I).

drop occurs within the first few seconds, reaching a shallow minimum by 30 s. A different response is seen in compound II, where the immediate current drop is smaller but does not seem to reach a stable value after 11 h. These observations are consistent with a picture of a nearly constant electronic current plus a transient ionic contribution during the bias pulse, followed by the ionic displacement back to equilibrium upon removal of the bias. The slight current increase beyond 30 s during the bias pulse in compound I can be attributed to enhanced electronic transport across the positively charged ionic layer at the cathode. However, this need not be a generic behavior of these materials.

The electronic conductivity may be taken as given by the final steady value of the current during the bias pulse (with caution due to the possibility of non-ohmic electrode-sample contacts). As seen from Fig. 6, a value of the order of 1.53 μS/cm is reasonable in compound I. In compound II, no steady current level is reached after 11 h; therefore, only an upper limit of 2.8 nS/cm can be given for the electronic conductivity.

References

[1] M.G. Kanatzidis, R. Bissessur, D.C. DeGroot, J.L. Schindler, C.R. Kannewurf, Chem. Mater. 5 (1993) 595.
[2] P. Aranda, E. Ruiz-Hitzky, Chem. Mater. 4 (1992) 1395.
[3] E. Ruiz-Hitzky, P. Aranda, B. Casal, J. Mater. Chem. 2 (1992) 581.
[4] E. Ruiz-Hitzky, R. Jimenez, B. Casal, V. Manríquez, A. Santa Ana, G. González, Adv. Mater. 5 (1993) 738.
[5] L.F. Nazar, H. Wu, W.P. Power, J. Mater. Chem. 5 (1995) 1985.
[6] I. Lagadic, A. Léaustic, R. Clément, J. Chem. Soc., Chem. Commun. (1992) 1396.
[7] R. Brec, D.M. Schleich, G. Ouvrard, A. Louisy, J. Rouxel, Inorg. Chem. 18 (1979) 1814.
[8] A. Le Mehaute, G. Ouvrard, R. Brec, J. Rouxel, Mater. Res. Bull. 12 (1977) 1191.
[9] V. Manríquez, A. Galdámez, J. Ponce, I. Brito, J. Kasaneva, Mater. Res. Bull. 34 (1999) 123.
[10] V. Manríquez, A. Galdámez, A. Villanueva, P. Aranda, J.C. Galván, E. Ruiz-Hitzky, Mater. Res. Bull. 34 (1999) 673.
[11] R. Clément, O. Garnier, J. Jegoudez, Inorg. Chem. 25 (1986) 1404.
[12] Y. Mathey, R. Clément, C. Sourisseau, G. Lucazeau, Inorg. Chem. 19 (1980) 2773.
[13] M.A. Ratner, D.F. Shriver, Chem. Rev. 88 (1988) 109.
[14] B.A. Boukamp, Equivalent Circuit Program, University of Twente, 1989.
[15] C.S. Hsu, F. Mansfeld, Corrosion 57 (2001) 747.
[16] J.T.S. Irvine, D.C. Sinclair, A.R. West, Adv. Mater. 2 (1990) 132.